Epilepsy Research (2010) xxx, xxx–xxx

journal homepage: www.elsevier.com/locate/epilepsyres

Predicting white matter targets for direct neurostimulation therapy

Marvin A. Rossi[a,*], Glenn Stebbins[a], Christopher Murphy[a], David Greene[b], Spencer Brinker[a], David Sarcu[a], Aaron Tenharmsel[a], Travis Stoub[a], Michael A. Stein[a], Thomas J. Hoeppner[a], Richard W. Byrne[a], Michael E. Moseley[c], Roland A. Bammer[c], Steve Bild[a], Jennifer Dennis[a], Nichole Arnett[a], Antoaneta Balabanov[a], Donna Bergen[a], Andres M. Kanner[a], Michael C. Smith[a]

[a] *Department Neurological Sciences, Rush University Medical Center, Chicago, IL, USA*
[b] *NeuroPace, Inc, Mountain View, CA, USA*
[c] *Department of Radiology, Stanford University, Palo Alto, CA, USA*

Received 25 February 2009; received in revised form 6 July 2010; accepted 18 July 2010

KEYWORDS
Deep brain stimulation;
Tractography;
Refractory epilepsy;
Parahippocampal gyrus;
Ictal propagation

Summary A novel depth electrode placement planning strategy is presented for propagating current to distant epileptic tissue during direct neurostimulation therapy. Its goal is to predict optimal lead placement in cortical white matter for influencing the maximal extent of the epileptic circuit. The workflow consists of three fundamental techniques to determine responsive neurostimulation depth lead placement in a patient with bilaterally independent temporal lobe epileptogenic regions. (1) Pre-implantation finite element modeling was used to predict the volume of cortical activation (VOCA). This model estimated the electric field and neural tissue influenced surrounding two adjacent active depth contacts prior to implantation. The calculations included anticipated stimulation parameters. (2) Propagation of stimulation therapy was simulated pre-implantation using the VOCA model positioned in the subject's diffusion tensor imaging (DTI) determined 8 h post-ictally compared to an interictal DTI. (3) Validation of the predicted stimulated anatomical targets was determined 4.3 months post-implantation using subtracted activated SPECT (SAS). Presurgically, the modeling system predicted white matter connectivity and visual side-effects to stimulation. Post-implantation, SAS validated focal blood flow changes in ipsilateral occipital and frontal regions, and contralateral temporal lobe. This workflow demonstrates the feasibility of planning white matter–electrode placement with individual specificity to predict propagation of electrical current throughout an epileptic circuit.

* Corresponding author at: Department Neurological Sciences, Rush University Medical Center, Rush Epilepsy Center, 1653 W. Congress Parkway, Suite 334 Murdock Building, Chicago, IL 60612, USA. Tel.: +1 312 942 5939; fax: +1 312 942 2238.
E-mail address: marossi@usa.net (M.A. Rossi).

0920-1211/$ – see front matter © 2010 Elsevier B.V. All rights reserved.
doi:10.1016/j.eplepsyres.2010.07.010

Introduction

Deep brain stimulation (DBS) (Medtronic, Minneapolis, MN) and responsive neurostimulation (RNS™ System, NeuroPace®, Inc. Mountain View, CA) are two investigational technologies seeking Food and Drug Administration (FDA) approval as adjunctive therapies in individuals with pharmacologically resistant localization-related epilepsy. The FDA recently recommended approval of DBS in the anterior nucleus of the thalamus as adjunctive therapy with severe and refractory partial-onset seizures with or without secondary generalization. DBS is a well-established treatment strategy for Parkinson's disease (Obeso et al., 2001), dystonia (Vidailhet et al., 2005; Kiss et al., 2007) and essential tremor (Benabid et al., 2009). Its use in the Stimulation of the Anterior Nucleus of the Thalamus Trial for Epilepsy (SANTE) utilizes a so-called open-loop stimulation delivery schedule. Specifically, stimulation current is intermittently delivered without feedback through bilateral depth electrode leads implanted stereotactically in the anterior nucleus of the thalamus (Hodaie et al., 2002). Conversely, efficacy of the NeuroPace® RNS™ System has been recently assessed in a multi-center pivotal clinical trial. This technology capitalizes on a closed-loop approach. That is, delivery of direct stimulation is contingent upon detecting the electrographic seizure onset. The stimulation parameters used by the implantable pulse generators (IPG) in both trials have been reached by trial-and-error. The neurostimulation paradigm for the DBS has been borrowed from its use in movement disorders, and that for the RNS™ System initially taken from after discharge study paradigms (Lesser et al., 1999). Nevertheless, recently presented clinical efficacy data for the SANTE and RNS™ System trials are promising (Fisher et al., 2010; Morrell et al., 2008, 2009).

A critical first step toward effectively applying direct brain stimulation therapy in epilepsy is to interface with the epileptic neural circuit. Epileptogenic cortex can include pathways that connect distant modulatory territories such as thalamus and pathological cortical regions (Luders et al., 2004). The term, 'epileptic focus' becomes a misnomer when such epileptic circuits are discussed. What remains unclear is how local stimulation can modulate potentially distant communicating epileptic tissue that may involve both cortical and subcortical regions.

Proposed mechanisms explaining acute-onset efficacy of local neurostimulation therapy include, conduction blockade (Beurruer et al., 2001), synaptic inhibition (Dostrovsky et al., 2000), synaptic depression (Urbano et al., 2002) and overriding pathophysiological neural network activity (Montgomery and Baker, 2000; Fukuda et al., 2001; Mcintyre et al., 2004; Zumsteg et al., 2006). In addition, chronic exposure to direct neurostimulation has been associated with distant cortical synaptic proliferation (Keller et al., 1992). Conversely, the possibility of enhancing pathological synaptic transmission cannot be ignored. Direct neurostimulation can acutely provoke the already hyperexcitable neural network. Moreover, well-established animal models demonstrate that chronic local delivery of specific stimulation parameters can produce secondary epileptogenesis (McIntyre and Goddard, 1973; VanLandingham and Lothman, 1991). Therefore, a substantial range of factors must be considered in the clinical response to stimulation delivered directly to neuronal populations. These variables include the number and interdependence of anatomical targets, electrode number, electrode location and orientation, geometry or shape of the electrode contacts, stimulation parameter settings (Butson et al., 2007), distribution of cathode and anode (Durand and Bikson, 2004), and the biophysical properties of stimulated medium compartments.

The goal of the depth electrode placement planning workflow developed in this study is to establish the feasibility of predicting with individual specificity, distant activation sites within the epileptic circuit communicating via white matter tracts. We hypothesize that it is possible to control the extent of neural tissue influenced in the mesial temporal regions using direct neurostimulation. Recently published data reveal that therapeutic direct stimulation in mesial temporal epilepsy consistently target hippocampal grey matter regardless of surrounding sclerosis (Velasco et al., 2000, 2001; Vonck et al., 2002; Tellez-Zenteno et al., 2006; Boon et al., 2007). An alternative approach is lead placement at the grey–white junction to allow the same depth lead to deliver therapeutic current to white matter propagation pathways while detecting the ictal onset in grey matter. Our center has successfully implanted investigational RNS™ System depth electrodes in juxtacortical epileptic mesial temporal white matter since 2004 (unpublished data). Parahippocampal white matter has robust afferent and efferent hippocampal pathways (Lavenex et al., 2007). Our goal has been to enhance propagation to distant epileptic tissue through white matter tracts. Achieving such activation using two four-contact RNS™ System leads may be improved with patient-specific placement planning. A presurgical workflow has evolved from this experience at Rush University Medical Center (RUMC) with the objective of maximally activating the epileptic network with therapeutic stimulation.

Methods

Three techniques are described in this study and treated individually as computationally intensive modules systematically implemented in a unique workflow (Fig. 1). The first two modules were employed prior to depth lead implantation. The algorithms were utilized to plan optimal depth lead placement in white matter adjacent to the epileptic region identified in the standard of care presurgical evaluation. The initial module, subtracted post-ictal diffusion tensor imaging (spiDTI), was used to assess anatomically specific changes in fractional anisotropy (FA) compared to baseline axonal water diffusion during the early post-ictal period of a focal-onset complex partial seizure. The spiDTI module composed the core of our depth lead planning system. The second of the three principal modules employed finite element method (FEM) modeling to predict the maximal electric field magnitude immediately surrounding active cylindrical depth contacts. The volume of cortical activation (VOCA) was calculated from the greatest magnitude of the electric field immediately surrounding the active contacts. In effect, the VOCA as used in this study was composed of juxtacortical white matter. We assumed constant and uniform bulk conductivities for isotropic white and grey

Please cite this article in press as: Rossi, M.A., et al., Predicting white matter targets for direct neurostimulation therapy. Epilepsy Res. (2010), doi:10.1016/j.eplepsyres.2010.07.010

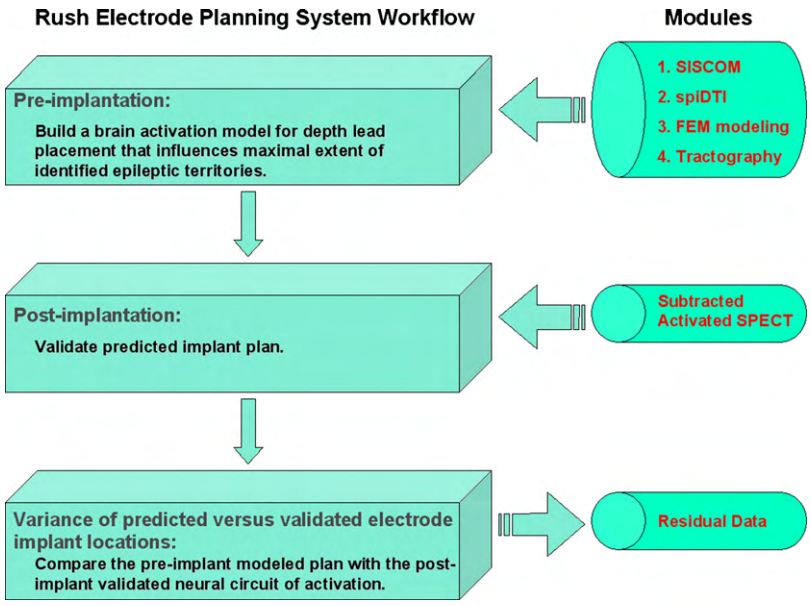

Figure 1 Block diagram illustrating system workflow and modules comprising the presurgical RNS depth lead implantation system developed at our center. SpiDTI = subtracted post-ictal diffusion tensor imaging, SISCOM = subtracted Ictal SPECT co-registered to MRI, FEM = finite element method.

matter compartments. Post-implantation, a final module, descriptively named subtracted activated SPECT (SAS), was utilized. This strategy utilizes an ability to indirectly measure focal neural activation (Rossi et al., 2008). This strategy was essential to validating the predicted white matter circuit actually activated by the given stimulation parameters, electrode location and lead orientation.

Subject

TS was a 20-year-old right-handed young woman at the time of surgery with acquired bilaterally independent temporal lobe epileptogenic regions. At the age of 5 years, she underwent a right middle temporal gyrus topectomy of a low-grade glioma followed by radiation treatment. At age 13, she began experiencing staring spells with an alteration in awareness, in addition to independent prolonged episodes of nausea and vomiting. Post-ictally, dizziness, unsteadiness and mild confusion typically lasted from hours to a day. At age 19, video-EEG monitoring revealed a prominent symptomatogenic epileptic region in the right neocortical temporal region clinically associated with severe nausea and vomiting. Electrographically, prolonged right peri-sylvian rhythmical delta range activity was correlated with the semiology. The onset of this seizure type was concordant with a subtracted ictal SPECT co-registered to MRI (SISCOM). A second seizure type captured by video-EEG monitoring was typical of her episodic staring spells with loss of awareness in the absence of an aura and without generalization secondarily. Electrographically, the ictal onset was associated with a buildup of left basal temporal rhythmical theta range slowing. No prior intracranial electrocorticography (ECoG) recording was performed. Since TS has active bilateral independent temporal lobe epileptic sources, she was not a candidate for epilepsy resective surgery, but qualified for the RNS™ System Pivotal Clinical Trial. The protocol described herein and the multi-center RNS™ System Pivotal Clinical Trial were both approved by the RUMC Institutional Review Board. TS voluntarily enrolled in both studies.

Subtracted post-ictal diffusion tensor imaging (spiDTI)

DTI sequences were acquired as diffusion weighted single shot spin echo. Echo planar images were axially acquired with the following parameters: TR/TE = 12100/97 ms, field of view = 25 cm, matrix = 128 × 128, 383 mm gapless slices, 6 repetitions, in plane resolution = 1.95 mm. Two diffusion weights (b-values) were used: $b = 0$ and 800 s/mm^2. The high b-value was obtained by applying diffusion encoding gradients along 24 non-collinear directions. This acquisition scheme was repeated six times for each slice, with the sign of all the gradient directions inverted for every other repetition. This acquisition scheme overcomes the inherent variance of DTI acquisitions during the scanning session. An additional set of inversion recovery images with cerebrospinal fluid nulling (TI ∼ 2100 ms) was acquired for each slice with $b = 0$ s/mm^2. These images were used to unwarp the eddy current effect of the diffusion gradients (de Crespigny and Moseley, 1998).

Comparisons of the interictal and post-ictal DTI datasets were determined for whole brain as follows. The post-ictal high resolution DTI dataset was acquired, where six repetitions of the DTI sequence were averaged for the same scanning session, exactly 8 h following the last seizure. The post-ictal phase is defined here as residual motor and sensory deficits (Todd's phenomenon) following a stereotypic seizure. A separate session was used to acquire the interictal DTI dataset, where the last documented complex partial seizure occurred 4 days prior. The same GE 1.5 T MR scanner with an LX Horizon high-speed gradient upgrade was used for both sessions. The two data sets were subtracted from each

Please cite this article in press as: Rossi, M.A., et al., Predicting white matter targets for direct neurostimulation therapy. Epilepsy Res. (2010), doi:10.1016/j.eplepsyres.2010.07.010

other and co-registered to the subject's 3D Fourier transform spoiled gradient recalled (SPGR) MR sequence (124 axially acquired 1.6 mm slices, 256 mm × 256 mm field of view and 0.85937 mm^3 isotropic voxels) in SPM5. Regions of interest in the subtracted DTI dataset were identified as those falling outside one standard deviation of the mean subtracted FA values.

Pre-implantation electric field modeling

Predicting the VOCA directly surrounding RNS cylindrical depth electrode contacts was calculated presurgically in anticipation of stereotactically placing the lead in left basal temporal white matter of subject TS. The depth lead was modeled according to the specifications of the actual electrode lead used in the clinical trial. Specifically, the model consisted of four conductive cylinders (1.27 mm diameter × 2 mm height) separated by insulators (10 mm between the midpoints of the conducting cylinders). The platinum/iridium electrode contact conductivity was set to 15×10^6 S/m. White matter was represented as a homogeneous and isotropic tissue medium (conductivity = 0.15 S/m). Adjacent isotropic grey matter conductivity was set to 0.06 S/m (Andreuccetti et al., 2005; Gimsa et al., 2004).

Preprocessing of the neuroimaging data was performed prior to importing the data in COMSOL Multiphysics v3.4 (Comsol Inc, Burlington, MA) for solving the VOCA solution as follows. Segmentation of grey and white matter was performed using Freesurfer for two acquired SPGR gapless MRI sequences where motion correction was applied (Dale et al., 1999). These segmented regions were flood-filled with solid colors. A finite element brain mesh was generated from this dataset using ScanIP (v2.1, Simpleware, LTD). For simplicity, the brain was modeled as two isotropic compartments (grey and white matter). These data were imported into COMSOL and converted to a composite of the grey and white matter geometry objects. The depth electrode model was positioned in the temporal white matter geometry object within 4–5 mm of the white–grey matter interface. The posterior two cylindrical contacts were placed in the left paramesial temporal region through the region of decreased mean FA as measured by spiDTI. The anterior tip of the electrode lead was located at the amygdala-hippocampal border. These electrode coordinates were coupled to the generated brain mesh in COMSOL. Such coupling within a common workspace allowed for iterative repositioning of the modeled electrode contacts. This composite model was generated using 234,237 geometry elements. Data processing was performed on an XP-based 64-bit dual quad core workstation with 64 gigabytes of RAM.

The Poisson equation solved with an efficient Fourier FEM solver (UMFPACK) within COMSOL was employed to model the electric field generated during bipolar stimulation of the two posterior depth contacts. A stimulation current was chosen within a therapeutic range used for those subjects implanted with at least one RNS™ System depth lead with mesial temporal epileptic sources. Therefore, a peak-to-peak potential difference of 5 Volts (V) from cathodic-to-anodic phases was measured using a digital storage oscilloscope (Alazar Technologies, Kirkland, QC) to generate a programmed constant stimulus current of 4.5 mA across a 500 Ω load-resistance in isotonic saline. In addition, the constant current neurostimulator was programmed with a 160 μs pulse width and a 100 ms burst duration delivered at 200 Hz. These settings generated a calculated charge density = 9.1 $\mu C/cm^2$ delivered to the two cylindrical electrode contacts with opposite polarities. For simplicity, time dependence was omitted from the calculations. The measured potential difference was used as an electrostatic scalar V to calculate the electric field (E) in a homogeneous isotropic medium, where, $E = -\text{gradient}(V)$.

The VOCA solution as derived from the maximum electric field magnitude was used to seed the patient's DTI for anticipated placement of the depth lead contacts. Expected white matter bundles recruited were modeled by diffusion tensor tractography using these seed regions of interest (ROI). The active bundles were estimated by examining the principal diffusion direction of adjacent voxels using a deterministic tracking algorithm from a continuous tensor field of the tensor elements (MR VISTA; http://white.stanford.edu/software).

Post-implant validation by subtracted activated SPECT

The final SAS module of the workflow was used to validate the presurgically modeled VOCA and white matter propagation circuit. This process was implemented 4.3 months following stereotactic implantation of the depth lead longitudinally in left temporal white matter. An occipital approach was used employing a Stealth navigational system (Medtronic, Inc.). In addition, a four-contact subdural strip was positioned in the right posterior superior temporal gyrus. The same implanted contacts were used for both eCoG recording and delivering stimulation therapy. The neurostimulator generator was implanted in the skull.

The stimulation parameters used in the presurgical simulation were actually delivered during post-implantation testing through posterior depth contacts 3–4 in a bipolar configuration while capturing resulting transient blood flow changes. The peripheral intravenous injection of a 5 cc bolus of ^{99}Tc-HMPAO was completed during delivery of six high frequency stimuli (200 Hz) at approximately 2 s intervals. The activated SPECT dataset was normalized and subtracted from a baseline SPECT using Analyze® v7.0 (AnalyzeDirect, Rochester, MN). ECoG did not capture seizures for 24 h prior to acquisition of the baseline SPECT. The SAS, post-implant CT (1 mm slice thickness, 168 contiguous axially acquired slices on a GE LightSpeed® scanner), and SPGR MR datasets were co-registered using the ITK co-registration algorithm in Analyze.

Results

Subtracted post-ictal diffusion tensor imaging

SpiDTI demonstrated a decrease in subtracted mean FA following a stereotypic complex partial seizure without generalization secondarily. A maximal difference was seen in left mesial temporal lobe white matter and corpus callosum. Specifically, a crescent-like signal was seen in the left paramesial temporal region that included parahippocampal

Please cite this article in press as: Rossi, M.A., et al., Predicting white matter targets for direct neurostimulation therapy. Epilepsy Res. (2010), doi:10.1016/j.eplepsyres.2010.07.010

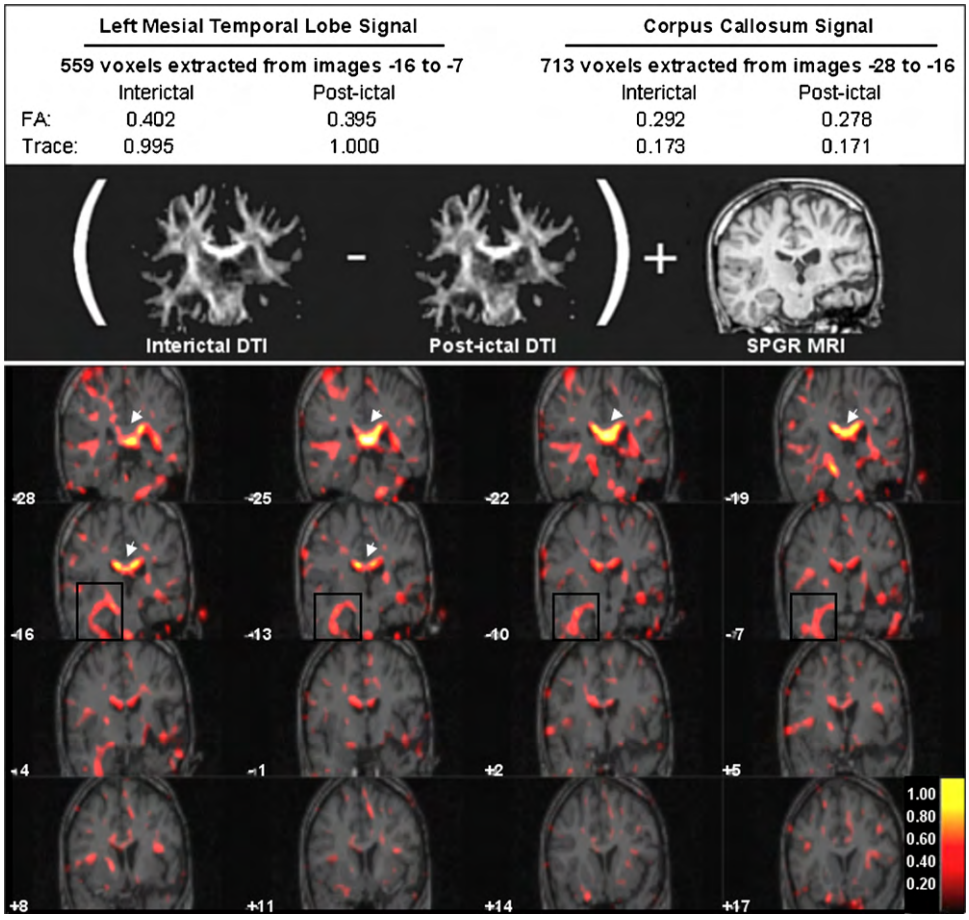

Figure 2 The spiDTI study is shown for subject TS. This technique demonstrates the post-ictal change in FA obtained exactly 8 h following a stereotypic complex partial seizure without generalization secondarily compared to a baseline DTI study. Note the maximal change in FA seen as a crescent-like signal in the left paramesial temporal region (black boxes) and corpus callosum (arrows). Images are neurologically oriented.

white matter. The corpus callosum signal was contiguous with the posterior superior temporal gyrus white matter. The mid-to-posterior corpus callosum showed the overall greatest post-ictal change in FA compared to baseline (Fig. 2).

Pre-implantation electric field modeling

A first approximation of predicting the stimulation-related VOCA was performed in a homogeneous isotropic medium representing white matter. Post-processing of the electric field solution was visualized in COMSOL as a 3D isosurface plot. The electric field strength within the modeled VOCA was measured along a transept line placed radially through the electrode contact center (Fig. 3C). A VOCA of 220 mm^3 was calculated surrounding each of the two active cylindrical electrode contacts defining the maximal electric field strength of 0.9—1.0 mV/mm expected to activate neuronal axons. This force estimate was taken from previously published data of neuronal activation cable models (Butson and McIntyre, 2005, 2006; Butson et al., 2007). This assumption was used as a first approximation to understand if this field strength estimate from the published literature could be extrapolated to model activation of axonal pathways of a cortical neuronal circuit. As expected, the strength of the modeled electric field decreased inversely proportional to the square of the field's radius (Astrom et al., 2006). The maximal field strength of 0.9—1.0 mV/mm resulted in the electric field's maximal magnitude radius of 3.75 mm from shaft center (3.12 mm from electrode surface; see Fig. 3D). A distance of 5 mm from the grey matter boundary was beyond the reach of the electric field's neural activation radius. Therefore, the boundary of the electric field's maximal magnitude overlapping the VOCA was assumed to remain in white matter with a constant conductivity. The electric field did not extend to grey matter where the change in conductivity would have deformed the spherical electric field volume. For simplicity, inhomogeneities of the fringe field at the edges of the electrode contacts were not considered (Fig. 3C and D, arrows).

This VOCA model was positioned within the spiDTI that captured maximal mean FA changes following a stereotypic left mesial onset seizure without generalization secondarily. The model was within our DTI voxel resolution of 1.95 mm × 1.95 mm × 3 mm. The spherical model was placed in a crescent-like signal in left paramesial temporal lobe white matter (Fig. 4B). The depth lead model was oriented longitudinally in inferior temporal lobe white matter that included the parahippocampal region. The calculated tractography model simulated the extent of white matter

Please cite this article in press as: Rossi, M.A., et al., Predicting white matter targets for direct neurostimulation therapy. Epilepsy Res. (2010), doi:10.1016/j.eplepsyres.2010.07.010

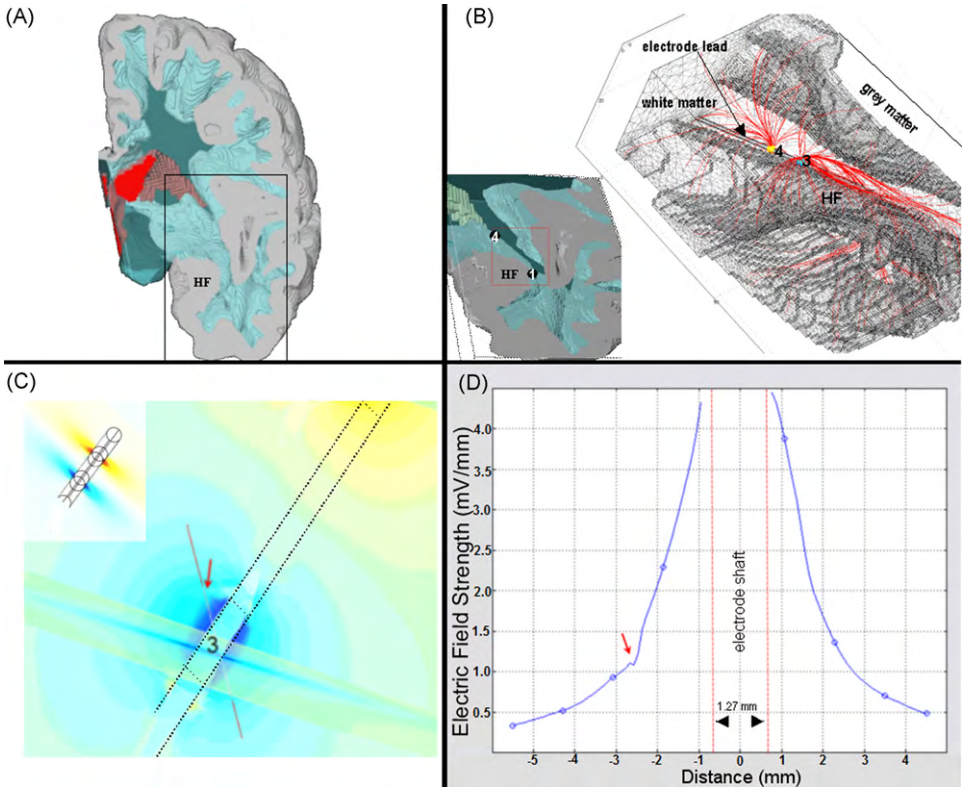

Figure 3 (A) Pre-implant patient-specific rendering of the white matter (transparent blue) and grey matter of the left mesial temporal region containing the hippocampal region (HF) for subject TS. The lateral ventricle is shown in red. Three-dimensional rendering of the hemisphere is neurologically oriented. (B) The anticipated electrode implant site is seen (arrow) near the HF grey—white matter junction. The inset illustrates anticipated orientation of the 4-contact depth lead. Electric field lines are modeled around contacts 3 (blue [cathode]) and 4 (yellow [anode]). The radial strength of the generally symmetric electric field was modeled as isosurfaces (C) with a radius of 3.75 mm from shaft center (midline between parallel red dotted lines) (D). Sudden transient drops of the electric field (red arrow in C and D) are seen near the fringes of the electric field surrounding the active contacts.

trajectories activated during delivery of direct stimulation via a depth electrode. These white matter pathways included: (1) ipsilateral optic radiation tracts projecting to the left occipital lobe, (2) a temporofrontal pathway ending in the left basal frontopolar region and (3) a projection to the contralateral posterior superior temporal gyrus confluent with the posterior corpus callosum (Fig. 4C and D).

An RNS™ System subdural four-contact electrode strip was planned for placement in contralateral superior temporal gyrus near a right temporal seizure-associated SISCOM region of transient hyperperfusion. Co-registration of this signal using SPM5 showed that it abutted a mean change in FA following a contralateral mesial temporal onset seizure (Fig. 6A). The spiDTi signal was confluent with the posterior corpus callosum. This multimodal neuroimaging overlay suggests communication between contralateral epileptic sources by way of the mid-to-posterior corpus callosum.

Post-implant validation

A SAS study acquired during stimulation of posterior depth contacts 3—4 demonstrated transient hypoperfusion-related changes beyond the immediately surrounding tissue. No after discharge was recorded at the site of stimulation as recorded by ECoG. Therefore, these transient hypoperfusion-related changes were due to direct stimulation itself and not by epileptiform activity. These data suggest communication with ipsilateral occipital and frontal cortices as well as contralateral neocortical temporal grey matter (Fig. 5C). Overlap of the SAS data with the recalculated post-implant tractography is shown in Fig. 5D using the VOCA solution as seed ROI centered around the CT co-registered depth contacts 3—4.

The proof of principle is demonstrated electrophysiologically in Fig. 6C where an ECoG obtained by the RNS™ System demonstrates propagation between epileptic sources interconnected by white matter pathways. Furthermore, clinical correlation of a reproducible visual response of elementary flashes of light in the superior visual fields subjectively reported by TS is associated with bipolar stimulation of posterior mesial temporal depth contacts 3—4. This sensory response corroborates propagation to primary visual or temporal association cortex predicted pre-implantation.

Discussion

We used a novel computationally intensive approach to predict targeted propagation of electrical current, prior to

Please cite this article in press as: Rossi, M.A., et al., Predicting white matter targets for direct neurostimulation therapy. Epilepsy Res. (2010), doi:10.1016/j.eplepsyres.2010.07.010

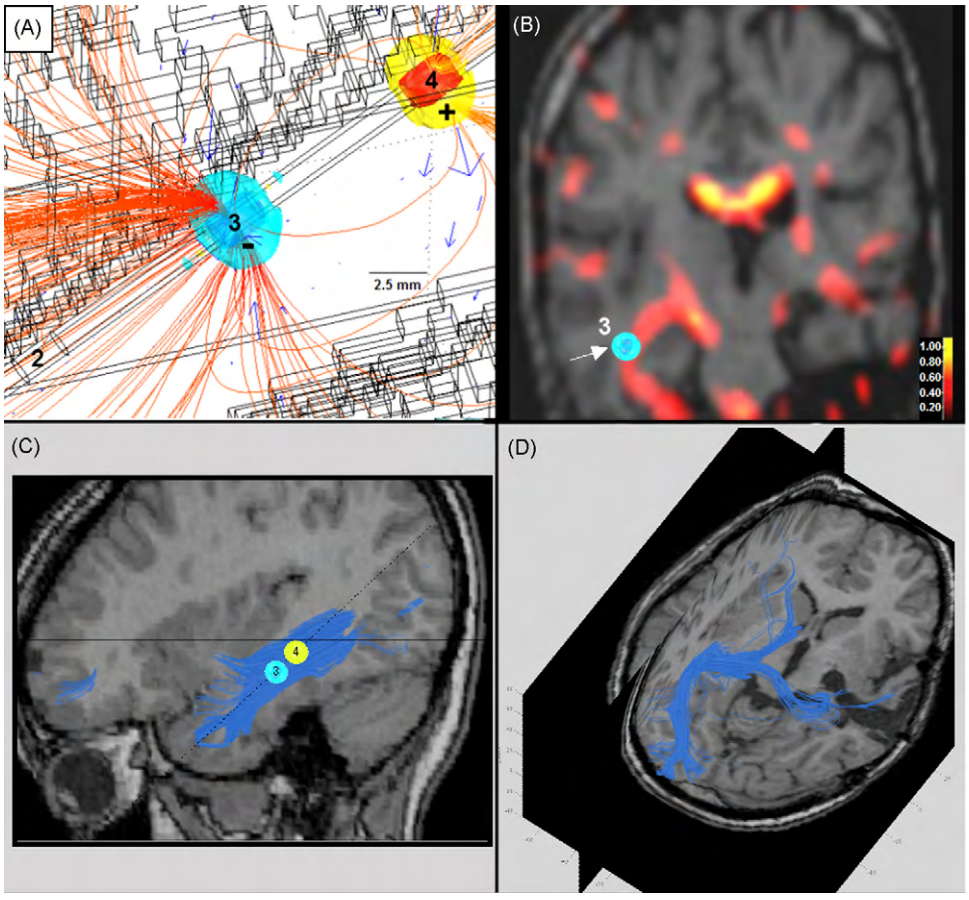

Figure 4 The pre-implant electrode stimulation-planning model is illustrated. (A) Delivery of bipolar stimulation to posterior depth contacts 3–4 (10 mm center–center) was modeled. The grey–white matter interface is represented by unsmoothed voxels (seen as cubes) using the MR SPGR data as displayed in COMSOL. (B) These ROI were positioned in the left temporal white matter overlapping the mean change in FA as measured by spiDTI (arrow). (C and D) The pre-implantation depth lead planning model represents the anticipated extent of white matter tracts influenced by stimulation. (C) The dotted line through the longitudinal axis of the hippocampal formation represents the anticipated trajectory for depth lead implantation. (D) The pre-implantation tractography model is shown for subject TS. Images are neurologically oriented.

stereotactically placing an RNS™ System depth lead at the grey–white matter junction in epileptic temporal white matter. Preoperatively, the maximal electric field gradient surrounding the active electrode contacts provided an estimate of the extent of cortical activation modeled during bipolar stimulation. The spatial extent of the neural response to an induced electric field has been previously calculated using the second spatial difference of the voltage distribution applied along the axon (Butson and McIntyre, 2005, 2006; Butson et al., 2007). Our conservative estimate of the VOCA model underestimated these calculations. However, unlike previously published unvalidated theoretical analyses, we validated the predicted tractography of activated axonal bundles post-implantation using SAS.

Pre-implantation modeling, as described here, relied on four fundamental assumptions as follows. Assumption 1: white and grey matter were assumed to be isotropic in our modeling calculations. This assumption was important as a first approximation for determining the maximal undistorted electric field density surrounding the active electrode contacts. Conductivity values of homogeneous white and grey matter used to calculate the electric field in this study were taken from published databases. Therefore, validation of these estimates was not performed with individual specificity. These values were determined based on a stimulation frequency of 200 Hz (Andreuccetti et al., 2005; Gimsa et al., 2004). This stimulation frequency is typically used for mesial temporal epileptic sources during the RNS Pivotal Clinical Trial. More sophisticated modeling can take into account tissue conductivity in a heterogeneous anisotropic tissue medium. For example, DTI can be used to predict the electrical conductivities of local brain tissue based on the supposition that DTI eigenvalues and electrical conductivity have a linear relationship in the human brain (Akhtari et al., 2006; Tuch et al., 2001). Such data can be validated *in vivo* in the operating room to provide accurate individual models of direct brain stimulation. Assumption 2: while the Poisson equation provides a spatial voltage solution, it does not account for the time dependence of the stimulus waveform or the capacitance of the electrode-tissue interface. Similar to the constant voltage circuit used by the Medtronic DBS IPG, the actual stimulus delivered to brain tissue by the constant current charging circuit of the RNS™ System neurostimulator may be modified by an interdependent

Please cite this article in press as: Rossi, M.A., et al., Predicting white matter targets for direct neurostimulation therapy. Epilepsy Res. (2010), doi:10.1016/j.eplepsyres.2010.07.010

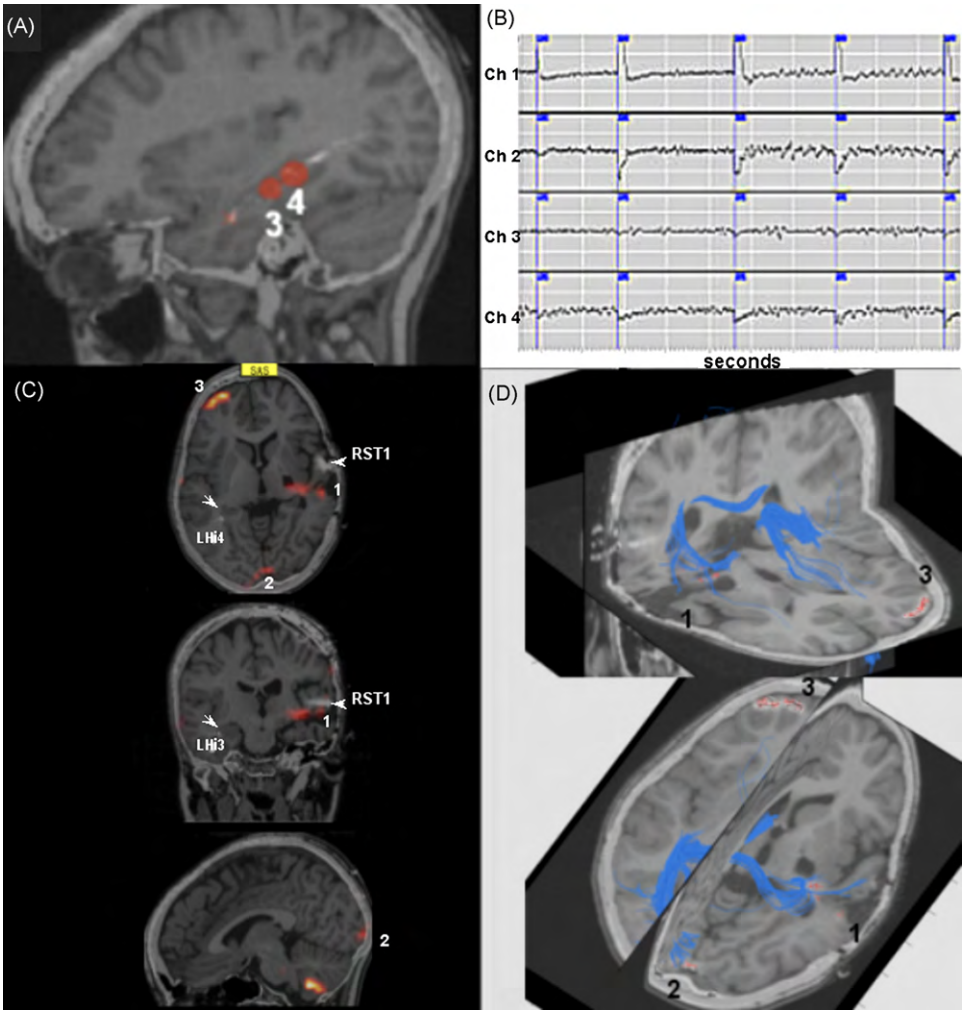

Figure 5 Post-implant validation of RNS current propagation pathways is shown. (A) The modeled electric fields with uniform radii are positioned to surround co-registered CT imaged depth contacts 3—4. These seed ROI were used to generate the post-implant tractography model of expected propagated RNS current. (B) No after discharge was recorded on ECoG during the delivery of 6 high frequency (200 Hz) stimuli at 0.4—0.5 Hz (blue lines) through all implanted electrode contacts using a bipolar configuration during activated SPECT acquisition (left hippocampal [LHi] depth lead: ch1-recording/stimulating through contacts 1—2, ch2-recording/stimulating through contacts 3—4; right superior temporal subdural [RST] strip: ch3-recording/stimulating through contacts 1—2, ch4-recording/stimulating through contacts 3—4.) (C) The three plane view of the SAS regions of transient hypoperfusion (labeled as 1—3) are shown co-registered with the post-implant CT (LHi depth contacts 3—4, and RST1 subdural contacts are shown). The recalculated post-implantation tractography model (blue) co-registered with the SAS regions of hypoperfusion (red) is shown (D).

tissue capacitance and impedance, which change slowly over time. An evolving capacitance is related to an encapsulation sheath surrounding the electrode lead (Mcintyre et al., 2004; Butson and McIntyre, 2005; Miocinovic et al., 2006). We assumed a constant 500 Ω electrode—tissue interface resistance without a capacitance. In our experience, such a resistance is within range of values returned by the RNS™ System impedance check during at least the first 6 months post-implantation. Furthermore, the neurostimulator is continuously regulated to maintain the programmed current. A compliance voltage of up to 14.3 V can be used to deliver current. Neural tissue only receives the voltage needed to drive the programmed current. A constant potential difference of 5 V peak-to-peak was assumed over the first 4 months post-implantation. Assumption 3: the electric field magnitude determined in our model was used to estimate a threshold value to activate a critical volume of white matter surrounding the electrode contacts. The electric field of interest surrounding each active contact was assumed to be undistorted and spherical. The 220 mm^3 volume of a static electric field geometry used to estimate the VOCA surrounding each electrode contact agreed with the previous literature (Mcintyre et al., 2004; Vasques et al., 2009). However, near-field regions at the cylindrical contact edges where the fringe electric field becomes complex were not considered in our calculations. A neuron exposed to these fringe fields can experience both inward and outward transmembrane currents, and, hence, regions of hyperpolarization and depolarization (Mcintyre et al., 2004). An ability to account for these effects was beyond the voxel resolution

Please cite this article in press as: Rossi, M.A., et al., Predicting white matter targets for direct neurostimulation therapy. Epilepsy Res. (2010), doi:10.1016/j.eplepsyres.2010.07.010

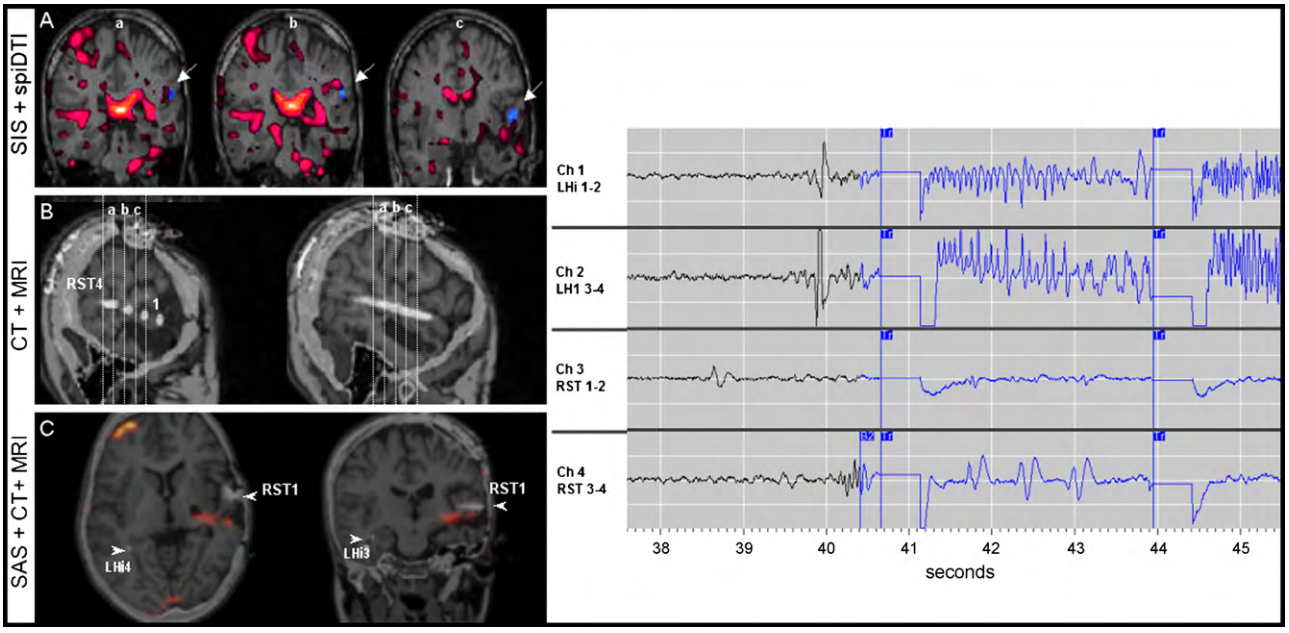

Figure 6 (A) A co-registration of a right neocortical temporal onset seizure captured by SISCOM (blue, arrow) and the mean difference in FA measured by spiDTI of a left mesial temporal onset seizure (coronal view from posterior to anterior). (B) The lateral view (sagittal cuts) of the post-implant CT co-registered with MRI is shown. The dotted lines demonstrate the coronal extent of the SISCOM signal. (C) Focal paroxysmal fast activity (B2) near the ictal onset was initially detected by RNS ECoG at the superior temporal subdural contacts (Ch4: RST3-4) (shown in B). Stimulation therapy (Tr) was set with the following parameters: current = 4.5 mA, pulse width = 160 μs, frequency = 200 Hz. Tr was delivered through all implanted electrode contacts and repeated at an interval of 3.5 s.

of our DTI protocol. Assumption 4: lastly, axon fibers oriented parallel to the active depth contacts were exposed to a larger voltage gradient and assumed to be preferentially activated in our model. An understanding of depth lead orientation is important for maximizing activation of surrounding white matter. Axons oriented predominantly in the direction of the voltage gradient are more likely to be activated, compared to axons oriented perpendicularly to the voltage gradient along isopotential lines (Rise, 2004).

SpiDTI provided the ability to determine the ratio of anisotropic (interictal mean FA) to isotropic (post-ictal mean FA) diffusion at the voxel level in relation to a stereotypic complex partial seizure without generalization secondarily. Diffusion-based imaging has been previously demonstrated to detect local changes in water diffusion in the early post-ictal period and during complex partial status epilepticus (Prichard et al., 1995; Zhong et al., 1997; Diehl et al., 2005; Salmenpera et al., 2006; Yogarajah and Duncan, 2008). DTI is based on the knowledge that the diffusion of water molecules within brain white matter is not equal in all directions. Molecular restriction is greater across axonal fibers than along the major axis. Intact brain white matter promotes anisotropic diffusion, whereas altered white matter post-ictally promotes isotropic diffusion (Prichard et al., 1995; Zhong et al., 1997). Therefore, post-ictal changes in FA of white matter pathways can be utilized to visualize the remnants of the directionality of a white matter circuit recruited by partial-onset seizures. These measures are not typically useful for those patients who experience secondarily generalized seizures. Propagation pathways become too complex to analyze. In our study, the mean diffusivity or trace, representing the overall free diffusion of water reflective of cell hydration, did not differ between the interictal and post-ictal DTI datasets. One factor explaining this finding may be due to the interval between seizure and post-ictal scanning (Salmenpera et al., 2006).

The presurgically modeled propagation map was validated post-implantation by utilizing SAS. Such a validation tool capitalizes on the coupling of blood flow changes with the metabolic demand placed on neuronal populations induced by electrical stimulation. Perfusion-related changes along with concordant clinical manifestations of direct cortical stimulation of mesial temporal white matter validate the presurgical cortical activation model. We have previously demonstrated discrete hypoperfusion-related changes both at the site of stimulation and propagated at a distance (Rossi et al., 2008). These findings are, in part, similar to previous reports of stimulation-related SPECT changes (Velasco et al., 2000). The underlying mechanisms explaining these changes are unknown. However, one hypothesis is that these local regions of transient hypoperfusion represent inhibitory activation, or suppressive communicating epileptic networks (Chkhenkeli et al., 2007).

Although limited to a single patient, the concordance of anticipated cortical activation targets with post-implant stimulation-related transient blood flow changes, ictal onset patterns measured by ECoG, and clinical side-effects to stimulation provide evidence that such electrode lead placement planning is feasible. These data further suggest that direct stimulation of white matter can be used to guide the spread of stimulation therapy to distant communicating neural targets. As a result, a greater extent of the epileptic circuit can be modulated with a minimal number of electrodes. In addition, stimulation induced side-effects

Please cite this article in press as: Rossi, M.A., et al., Predicting white matter targets for direct neurostimulation therapy. Epilepsy Res. (2010), doi:10.1016/j.eplepsyres.2010.07.010

can be predicted and, therefore, minimized with such preoperative planning.

Conclusions

Our preliminary data offer a proof of concept achieved for this computational modeling workflow to propose electrode implant location, orientation and basic stimulation parameters in temporal white matter. An influence on clinical efficacy, however, is yet to be determined. Assessment of seizure control for subject TS in the RNS™ System Pivotal Clinical Trial is currently in progress.

We have proposed a system to plan implantation sites and orientation for depth electrodes in juxtacortical white matter of the mesial temporal region. This electrode placement planning workflow may improve the probability of modulating the maximal extent of a bilateral temporal lobe epileptic network with a minimum of electrodes, and not simply the presumed grey matter 'focus'. A mechanistic interplay between cortical and subcortical structures, such as thalamus, may provide an incentive for future clinical trials combining stimulation of both regions. Development of this strategy will lead to a better understanding and clarity of individual differences seen with direct cortical stimulation delivered through white matter pathways to distant epileptic neural tissue. These data underscore the need to regard localization-related epilepsies as potentially extensive pathological neural networks.

Conflicts of interest

We confirm that we have read the Journal's position on issues involved in ethical publication and affirm that this report is consistent with those guidelines. D. Greene is an employee of NeuroPace Inc. He receives a salary and has stock options from NeuroPace, Inc. All remaining authors have no professional or financial affiliations that might be perceived as having biased the presentation. These authors have provided full disclosure of any conflict(s) of interest and have no conflicts of interest to disclose.

Acknowledgement

Support from NeuroPace, Inc. as well as RUMC departmental and institutional resources are gratefully acknowledged.

References

Akhtari, M., Salamon, N., Duncan, R., Fried, I., Mathern, G.W., 2006. Electrical conductivites of the freshly excised cerebral cortex in epilepsy surgery patients: correlation with pathology, seizure duration, and diffusion tensor imaging. Brain Topogr. 18, 281—290.

Andreuccetti, D., Fossi, R., Petrucci, C., 2005. Dielectric Properties of Body Tissue Italian Research Council. Institute for Applied Physics, Florence, Italy, http://niremf.ifac.cnr.it/tissprop.

Astrom, M., Johansson, J.D., Hariz, M.I., Eriksson, O., Wardell, K., 2006. The effect of cystic cavities on deep brain stimulation in the basal ganglia: a simulation-based study. J. Neurol. Eng. 3, 132—138.

Benabid, A.L., Chabardes, S., Mitrofanis, J., Pollak, P., 2009. Deep brain stimulation of the subthalamic nucleus for the treatment of Parkinson's disease. Lancet Neurol. 8, 67—81.

Beurruer, C., Bioulac, B., Audin, J., Hammond, C., 2001. High-frequency stimulation produces a transient blockade of voltage-gated currents in subthalamic neurons. J. Neurophysiol. 85, 1351—1356.

Boon, P., Vonck, K., De Herdt, V., Van Dycke, A., Goethals, M., Goossens, L., Van zandijcke, M., De SmeDt, T., Dewaele, I., Achten, R., Wadman, W., Dewaele, F., Caemaert, J., Van Roost, D., 2007. Deep brain stimulation in patients with refractory temporal lobe epilepsy. Epilepsia 48, 1551—1560.

Butson, C.R., McIntyre, C.C., 2005. Tissue and electrode capacitance reduce neural activation volumes during deep brain stimulation. Clin. Neurophys. 116, 2490—2500.

Butson, C.R., McIntyre, C.C., 2006. Role of electrode design on the volume of tissue activated during deep brain stimulation. J. Neurol. Eng. 3, 1—8.

Butson, C.R., Cooper, S.E., Henderson, J.M., McIntyre, C.C., 2007. Patient-specific analysis of the volume of tissue activate during deep brain stimulation. Neuroimage 34, 661—670.

Chkhenkeli, S.A., Towle, V.L., Lortkipanidze, G.S., Spire, J.-P., Bregvadze, E.S., Hunter, J.D., Kohrman, M., Frim, D.M., 2007. Mutually suppressive interrelations of symmetric epileptic foci in bitemporal epilepsy and their inhibitory stimulation. Clin. Neurol. Neurosurg. 109, 7—22.

Dale, A.M., Fischl, B., Sereno, M.I., 1999. Cortical surface-based analysis. I. Segmentation and surface reconstruction. Neuroimage 9, 179—194.

de Crespigny, A.J., Moseley, M.E., 1998. Eddy current induced image warping in diffusion weighted EPI. In: Abstr of the Int Soc of MR in Med. ISMRM, 6th Meeting. Sydney, Australia, Abstr 2661.

Diehl, B., Symms, M.R., Boulby, P.A., Salmenpera, T., Wheeler-Kingshott, C.A.M., Barker, G.J., Duncan, J.S., 2005. Postictal diffusion tensor imaging. Epilepsy Res. 65, 137—146.

Dostrovsky, J.O., Levy, R., Wu, J.P., Hutchison, W.D., Tasker, R.R., Lozano, A.M., 2000. Microstimulation-induced inhibition of neuronal firing in human globus pallidus. J. Neurophysiol. 84, 570—574.

Durand, D.M., Bikson, M., 2004. Control of neuronal activity by electric fields: in vitro models of epilepsy. In: Luders, H.O. (Ed.), Deep Brain Stimulation and Epilepsy. Martin Dunitz, London & New York, pp. 67—86.

Fisher, R., Salanova, V., Witt, T., Worth, R., Henry, T., Gross, R., Oomen, K., Osorio, I., Nazzaro, J., Labar, D., Kaplitt, M., Sperling, M., Sandock, E., Neal, J., Handforth, A., Stern, J., DeSalles, A., Chung, S., Shetter, A., Bergen, D., Bakay, R., Henderson, J., French, J., Baltuch, G., Rosenfeld, W., Youkilis, A., Marks, W., Garcia, P., Barbaro, N., Fountain, N., Bazil, C., Goodman, R., McKhann, G., Krishnamurthy, B., Papavassiliou, S., Epstein, C., Pollard, J., Tonder, L., Grebin, J., Coffey, R., Graves, N., 2010. Electrical stimulation of the anterior nucleus of thalamus for treatment of refractory epilepsy. Epilepsia 51, 899—908.

Fukuda, M., Mentis, M.J., Ma, Y., Moeller, J.R., Dhawan, V., Antonini, A., Lang, A.E., Lozano, A.M., Hammerstad, J., Lyons, K., Koller, W.C., Eidelberg, D., 2001. Networks mediating the clinical effects of pallidal brain stimulation for Parkinson's disease: a PET study of resting-state glucose metabolism. Brain 124, 2105—2118.

Gimsa, J., Habel, B., Schreiber, U., van Rienen, U., Strauss, U., Gimsa, U., 2004. Choosing electrodes for deep brain stimulation experiments—electrochemical considerations. J. Neurosci. Methods 142, 251—265.

Hodaie, M., Wennberg, R.A., Dostrovsky, J.O., Lozano, A.M., 2002. Chronic anterior thalamus stimulation for intractable epilepsy. Epilepsia 43, 603—608.

Keller, A., Arissian, K., Asanuma, H., 1992. Synaptic proliferation in the motor cortex of adult cats after thalamic stimulation. J. Neurophysiol. 68, 295—308.

Please cite this article in press as: Rossi, M.A., et al., Predicting white matter targets for direct neurostimulation therapy. Epilepsy Res. (2010), doi:10.1016/j.eplepsyres.2010.07.010

Kiss, Z.H.T., Doig-Beyaert, K., Eliasziw, M., Tsui, J., Haffenden, A., Suchowersky, O., 2007. The Canadian multicentre study of deep brain stimulation for cervical dystonia. Brain 130, 2879–2886.

Lavenex, P., Banta Lavenex, P., Amaral, D.G., 2007. Postnatal development of the primate hippocampal formation. Dev. Neurosci. 29, 179–192.

Lesser, R.P., Kim, S.H., Beyderman, L., et al., 1999. Brief bursts of pulse stimulation terminate after discharges caused by cortical stimulation. Neurology 53, 2073–2081.

Luders, J., Najm, I., Luders, H.O., 2004. Brain stimulation and epilepsy: basic overview and novel approaches. In: Luders, H.O. (Ed.), Deep Brain Stimulation and Epilepsy. Martin Dunitz, London & New York, pp. 3–17.

McIntyre, D.C., Goddard, G.V., 1973. Transfer, interference and spontaneous recovery of convulsions kindled from the rat amygdale. Electroencephalogr. Clin. Neurophysiol. 35, 533–543.

Mcintyre, C.C., Mori, S., Sherman, D.L., Thakor, N.V., Vitek, J.L., 2004. Electric field and stimulating influence generated by deep brain stimulation of the subthalamic nucleus. Clin. Neurophys. 115, 589–595.

Miocinovic, S., Parent, M., Butson, C.R., Hahn, P.J., Russo, G.S., Vitek, J.L., McIntyre, C.C., 2006. Computational analysis of subthalamic nucleus and lenticular fasciculus activation during therapeutic deep brain stimulation. J. Neurophys. 96, 1569–1580.

Montgomery, E.B., Baker, K.B., 2000. Mechanisms of deep brain stimulation and future technical developments. Neurol. Res. 22, 259–266.

Morrell, M.J., Hirsch, L.J., Bergey, G., Barkley, G., Wharen, R., Murro, A., Fisch, B., Rossi, M.A., Labar, D., Duckrow, R., Sirven, J.I., Drazkowski, J., Worrell, G.A., 2008. Long-term safety and efficacy of the RNS system in adults with medically-intractable partial onset seizures. Epilepsia 49 (s7), 480.

Morrell, M.J., Hirsch, L.J., Bergey, G., Barkley, G., Wharen, R., Murro, A., Fisch, B., Rossi, M.A., Labar, D., Duckrow, R., Sirven, J.I., Drazkowski, J., Worrell, G.A., Gwinn, R.P., 2009. Results of a Multicenter Double Blinded Randomized Controlled Pivotal Investigation of the RNS^{TM} System for Treatment of Intractable Partial Epilepsy in Adults. AES Abstr B09 (Platform).

Obeso, J.A., Olanow, C.W., Rodriguez-Oroz, M.C., Krack, P., Kumar, R., Lang, A.E., 2001. Deep-brain stimulation of the subthalamic nucleus or the pars interna of the globus pallidus in Parkinson's disease. N. Engl. J. Med. 345, 956–963.

Prichard, J.W., Zhong, J., Petroff, O.A., Gore, J.C., 1995. Diffusion-weighted NMR imaging changes caused by electrical activation of the brain. NMR Biomed. 8, 359–364.

Rise, M.T., 2004. Brain stimulation and epilepsy: electrical stimulus characteristics. In: Luders, H.O. (Ed.), Deep Brain Stimulation and Epilepsy. Martin Dunitz, London & New York, pp. 45–54.

Rossi, M.A., Hoeppner, T.J., Byrne, R.W., Greene, D., Kanner, A.M., Stoub, T., Stein, M.A., Balabanov, A., Bergen, D., Smith, M.C., 2008. Subtracted activated SPECT validates depth lead placement in white matter for responsive neurostimulation therapy in refractory partial-onset epilepsy. Epilepsia 49 (Suppl. 7), abstr 3.102, 355.

Salmenpera, T.M., Symms, M.R., Boulby, P.A., Barker, G.J., Duncan, J.S., 2006. Postictal diffusion weighted imaging. Epilepsy Res. 70, 133–143.

Tellez-Zenteno, J.F., McLachlan, R.S., Parrent, A., Kubu, C.M., Weibe, S., 2006. Hippocampal electrical stimulation in mesial temporal lobe epilepsy. Neurology 66, 1490–1494.

Tuch, T.S., Wedeen, V.J., Dale, A.M., George, J.S., Belliveau, J.W., 2001. Conductivity tensor imaging of the human brain using diffusion tensor MRI. Proc. Natl. Acad. Sci. 98, 11697–11701.

Urbano, F.J., Leznik, E., Llinas, R.R., 2002. Cortical activation patterns evoked by afferent axons stimuli at different frequencies: an *in vivo* voltage-sensitive dye imaging study. Thalamus Relat. Syst. 1, 371–378.

VanLandingham, K.E., Lothman, E.W., 1991. Self-sustaining limbic status epilepticus. II. Role of hippocampal commissures in metabolic responses. Neurology 41, 1950–1957.

Vasques, X., Cif, L., Hess, O., Gavarini, S., Mennessier, G., Coubes, P., 2009. Stereotactic model of the electrical distribution within the internal globus pallidus during deep brain stimulation. J. Comput. Neurosci. 26, 109–118.

Velasco, M., Velasco, F., Velasco, A.L., Boleaga, B., Jimenez, F., Brito, F., Marquez, I., 2000. Subacute electrical stimulation of the hippocampus blocks intractable temporal lobe seizures and paroxysmal EEG activities. Epilepsia 41, 158–169.

Velasco, M., Velasco, F., Velasco, A.L., Menez, D., Rocha, L., 2001. Electrical stimulation for epilepsy: Stimulation of hippocampal foci. Stereotact. Funct. Neurosurg. 77, 223–227.

Vidailhet, M., Vercueil, L., Houeto, J.L., Krystkowiak, P., Benabid, A.L., Cornu, P., Lagrangem, C., Tezenas du Montcel, S., Dormont, D., Grand, S., Blond, S., Detante, O., Pillon, B., Ardouin, C., Agid, Y., Destee, A., Pollak, P., 2005. Bilateral deep-brain stimulation of the globus pallidus in primary generalized dystonia. N. Engl. J. Med. 352, 459–467.

Vonck, K., Boon, P., Achten, E., DeReuck, J., Caemaert, J., 2002. Long-term amygdalohippocampal stimulation for refractory temporal lobe epilepsy. Ann. Neurol. 52, 556–565.

Yogarajah, M., Duncan, J.S., 2008. Diffusion-based magnetic resonance imaging and tractography in epilepsy. Epilepsia 49, 189–200.

Zhong, J., Petroff, O.A., Pleban, L.A., Gore, J.C., Prichard, J.W., 1997. Reversible, reproducible reduction of brain water apparent diffusion coefficient by cortical electroshocks. Magn. Reson. Med. 37, 1–6.

Zumsteg, D., Lozano, A.M., Wennberg, R.A., 2006. Mesial temporal inhibition in a patient with deep brain stimulation of the anterior thalamus for epilepsy. Epilepsia 47, 1958–1962.

Please cite this article in press as: Rossi, M.A., et al., Predicting white matter targets for direct neurostimulation therapy. Epilepsy Res. (2010), doi:10.1016/j.eplepsyres.2010.07.010